European Journal of Radiology 84 (2015) 1269–1276

Contents lists available at ScienceDirect

European Journal of Radiology

journal homepage: www.elsevier.com/locate/ejrad

Simultaneous PET/MR head–neck cancer imaging: Preliminary clinical experience and multiparametric evaluation

M. Covello[a,*], C. Cavaliere[a], M. Aiello[a], M.S. Cianelli[a], M. Mesolella[b], B. Iorio[b], A. Rossi[a], E. Nicolai[a]

[a] IRCCS SDN, Via E. Gianturco, 111-113 – 80143, Naples, Italy
[b] Department of Otorhinolaryngoiatry, Federico II University, Naples, Italy

ARTICLE INFO

Article history:
Received 17 March 2014
Received in revised form 26 March 2015
Accepted 11 April 2015

Keywords:
Hybrid imaging
PET/MR
SUV
DCE
DWI
Head and neck cancer

ABSTRACT

Purpose: To evaluate the role of simultaneous hybrid PET/MR imaging and to correlate metabolic PET data with morpho-functional parameters derived by MRI in patients with head–neck cancer.
Methods: Forty-four patients, with histologically confirmed head and neck malignancy (22 primary tumors and 22 follow-up) were studied. Patients initially received a clinical exam and endoscopy with direct biopsy. Next patients underwent whole body PET/CT followed by PET/MR of the head/neck region. PET and MRI studies were separately evaluated by two blinded groups (both included one radiologist and one nuclear physician) in order to define the presence or absence of lesions/recurrences. Regions of interest (ROIs) analysis was conducted on the primary lesion at the level of maximum size on metabolic (SUV and MTV), diffusion (ADC) and perfusion (K^{trans}, V_e, k_{ep} and iAUC) parameters.
Results: PET/MR examinations were successfully performed on all 44 patients. Agreement between the two blinded groups was found in anatomic allocation of lesions by PET/MR (Primary tumors: Cohen's kappa 0.93; Follow-up: Cohen's kappa 0.89). There was a significant correlation between CT-SUV measures and MR (e.g., CT-SUV VOI vs. MR-SUV VOI: $\rho = 0.97$, $p < 0.001$ for the entire sample). There was also significant positive correlations between the ROI area, SUV measures, and the metabolic parameters (SUV and MTV) obtained during both PET/CT and PET/MR. A significant negative correlation was observed between ADC and K^{trans} values in the primary tumors. In addition, a significant negative correlation existed between MR SUV and ADC in recurrent tumors.
Conclusion: Our study demonstrates the feasibility of PET/MR imaging for primary tumors and recurrent tumors evaluations of head/neck malignant lesions. When assessing HNC, PET/MR allows simultaneous collection of multiparametric metabolic and functional data. This technique therefore allows for a more complete characterization of malignant lesions.

© 2015 Elsevier Ireland Ltd. All rights reserved.

1. Introduction

Head and neck cancers (HNC) account for approximately 4–5% of all malignant disease. Of these, head and neck squamous cell carcinoma (HNSCC) comprises the vast majority (90%) [1]. Diagnosis of head and neck cancer is typically achieved by a combination of physical examination and either nasopharyngoscopy and/or laryngoscopy with direct biopsies. However, the first manifestation of the disease commonly involves the cervical lymph nodes, also the presence of distant metastases and different primaries must be considered. Following diagnosis, accurate staging is critical for selection of the appropriate treatment strategy. For early-stage disease, surgery or radiotherapy are the most common treatments, with a success rate of about 80% [2]. Postoperative radiotherapy is typically recommended when the risk for locoregional recurrence exceeds 20% [3]. For patients whose disease is not controlled with definitive radiotherapy, salvage surgery is recommended [3]. For regionally advanced HNSCC, concurrent chemo-radiotherapy has been widely used [4]. Currently, positron emission tomography (PET) and magnetic resonance (MR) are well-established imaging techniques for the staging [5] and follow-up of HNC. MR techniques, such as diffusion weighted imaging (DWI) and dynamic contrast enhancement (DCE), along with fluorodeoxyglucose (FDG)-PET are the basilar imaging techniques used to assess angiogenesis and metabolism in HNSCC. Development of noninvasive imaging biomarkers might assist in planning optimal treatment strategies,

* Corresponding author. fax: +39 081668841.
E-mail address: echoplanare@gmail.com (M. Covello).

http://dx.doi.org/10.1016/j.ejrad.2015.04.010
0720-048X/© 2015 Elsevier Ireland Ltd. All rights reserved.

which may lead to a more favorable therapeutic outcome [6,7]. The recent commercial introduction of hybrid PET/MR scanners offer new possibilities for oncologic imaging, combining the wide range of physiological information (glucose metabolism, cell proliferation, hypoxia, cell receptor expression) achievable by different PET tracers with the high spatial and contrast resolution of MRI. Moreover, advanced MRI techniques (DWI, DCE and MR spectroscopy) yield functional information that may complement the findings of PET imaging. To date, several PET/MRI studies have shown promising results for clinical oncologic applications [8,9]. The best applications for PET/MRI imaging exist for HNC. Due to the complex anatomy of this region the superb soft-tissue contrast resolution of MRI is extremely useful. For this reason, PET/MRI seems to be highly accurate in the evaluation of primary extension (T-staging). However, it has no significant benefit with lymph nodes involvement (N-staging) and limited improvement for metastasis detection (M-staging) when compared to PET/CT examination [10].

Therefore, the aims of the study were to evaluate feasibility of simultaneous hybrid PET/MR imaging in patients with HNC. In addition, metabolic data obtained from PET and morphologic and functional data (DWI, DCE) obtained by MRI on primary tumors and recurrent lesions were correlated. In this context, the new technology of simultaneous PET/MR scanning can be suitable for a comprehensive multiparametric assessment. We present our initial clinical experience with simultaneous PET/MR imaging in the evaluation of patients affected by HNC.

2. Materials and methods

2.1. Patient population and Imaging protocol

In accordance with the institutional review board and Ethical Committee, 44 consecutive patients (mean age 57 ± 12; 23 males and 9 females) with histologically confirmed head and neck malignancy (22 primary tumors and 22 recurrent tumors) were studied between March, 2012 to June, 2013. Exclusion criteria consisted of >150 mg/dL blood glucose, pregnancy, and standard contraindication for MRI. For primary tumors, no therapy has been started at the time of MR imaging. For recurrent lesions, imaging session has been performed 6–8 weeks after the end of treatment (including 12 patients treated with surgery, 4 with radiotherapy, and the remaining with a combination of surgery and radiotherapy). All patients underwent a one day single-injection imaging protocol including PET/CT and subsequent PET/MR.

Briefly, patients were fasted for at least 6 h before scanning, followed by blood glucose assessment prior to FDG injection. A dose of 406 ± 40 MBq of [18F]-FDG was injected based on the patient's body weight. Following an uptake period (81 ± 15 min), patients underwent a PET/CT scan. After completion of the PET/CT scan, patients then received a head and neck PET/MR examination.

2.2. PET/CT acquisition

PET/CT acquisition was performed on a Gemini TF (Philips Medical Systems, Best, The Netherlands) tomograph designed with a multi-ring LYSO block detectors system and a nominal axial resolution near the center of field of view of 4.8 mm (FWHM) with an absolute sensitivity of 6.6 kcps/MBq, as previously reported [11].

According to our routine protocol for oncological studies, PET data was acquired in sinogram mode for 15 min with amatrix size of 144×144. PET data were reconstructed using the LOR-TF-RAMLA algorithm, therefore data was post filtered with a three-dimensional isotropic gaussian of 4 mm at FWHM. CT-based attenuation maps were created with a low dose CT scan (120 kV, 80 mA) using commonly employed bi-linear scaling. The acquisition time was 3 min per bed position (BP), with 5\6 BPs (each 21 cm) covering the trunk of the patients starting from the pelvis and moved up toward the head. Following whole body acquisition an additional BP was acquired focusing on the head/neck region. The result was a total acquisition time of approximately 18mins per patient for PET/CT.

The patients were positioned supine with their arms brought together above the head for total body acquisition and with their arms resting at the sides for head/neck acquisition.

2.3. PET/MR Acquisition

PET/MR was performed on the Biograph mMR (Siemens Healthcare, Erlangen, Germany). This system consists of a 3 T MRI scanner featuring high-performance gradient systems (45 mT/m) and a slew rate of 200 T/m/s. The PET/MR system is equipped with Total Imaging Matrix coil technology (Siemens Healthcare), covering the entire body with multiple integrated radiofrequency surface coils. The coils, patient table, and cables have been redesigned for PET/MR in order to minimize their attenuation and to allow unimpaired PET acquisition with the coils in place. A fully functional PET system equipped with the avalanche photodiode technology is embedded into the magnetic resonance gantry.

The PET scanner has a spatial resolution of 4.1 mm (FWHM) at 1 cm and of 5.0 mm (FWHM) at 10 cm from the transverse FOV and a sensitivity of 11.72 kcps/MBq at the center of the FOV.

On average, the PET/MR scan started about 20 min after the start of the PET/CT acquisition. Bed position was established in order to get full coverage of the head/neck region. After correct positioning was established, the combined PET/MR acquisition was performed.

First, a coronal 2-point Dixon 3-dimensional volumetric interpolated breath-hold T1-weighted MRI sequence was acquired and used for the generation of attenuation maps and for anatomic allocation of the PET results. The software of the MRI scanner automatically generates 4 different images: T1-weighted in-phase, T1-weighted out-of-phase, water-only, and fat-only. Simultaneously with the start of the Dixon MRI sequence, PET acquisition began to ensure correct temporal and regional correspondence between MRI and PET data. The PET acquisition time was 4 min and considering simultaneous MR acquisition the total PET/MR examination lasted about 30 min.

2.4. PET data reconstruction

PET data obtained on the PET/CT and PET/MR scanners were processed with comparable reconstruction and correction algorithms. For both modalities, emission data were corrected for randoms, dead time, scatter, and attenuation. A 3-dimensional attenuation-weighted ordered-subsets expectation maximization iterative reconstruction algorithm (AW OSEM 3D) was applied with 3 iterations and 21 subsets, gaussian smoothing of 4 mm in full width at half maximum, and a zoom of 1. Attenuation maps were obtained from the CT data by bilinear transformation, as implemented in the post-processing software of the PET/CT scanner and were used for attenuation correction of the PET/CT data.

2.5. MRI-based attenuation correction

PET attenuation correction (AC) is a critical issue for integrated PET/MRI scanners. Contrarily to X-ray CT, which inherently provides a patient-specific measurement of the electron density, MRI signal is only related to proton density. Therefore, MRI is intrinsically unable to measure attenuation factors due to electron density. Proposed solutions are substantially based on the combination of custom-tailored MRI acquisitions with image processing, pattern recognition, and template-matching techniques.

In this work, clinically approved AC is performed by means of the attenuation maps generated on the basis of the 2-point Dixon MRI sequences obtained for every BP. This approach has recently been demonstrated to provide results comparable to those of conventional attenuation correction by low dose CT [12]. The procedure has been implemented in the post-processing software of the scanner and operates automatically. The Dixon fat- and water-weighted images were used to create an attenuation map with 4 distinct tissue-classes: background, lungs, fat, and soft tissue. Attenuation of the PET signal caused by instrumentation, such as the patient bed and the fixed MRI coils, is automatically integrated into the attenuation maps [13].

It is worth noting that such AC approach ignores the presence of bony structures, therefore limiting quantitative accuracy in anatomical districts containing (or close to) bones [14]. To address this issue, more refined AC techniques are currently under investigation and clinical validation [15].

2.6. MR acquisition

The MRI protocol was performed with a dedicated 16 channel head and neck coil including: coronal STIR, axial FSE T2-weighted, axial FSE T1-weighted, axial diffusion-weighted imaging (DWI), and a single-shot echo planar 2D SPAIR. In this sequence three b values were applied: 0, 500 and 800 s/mm^2.

Perfusion studies were dynamically acquired immediately after intravenous administration of paramagnetic contrast (Magnevist®, Bayer-Schering, Berlin, Germany) with 50 measurements of volume Interpolated GRE preceded by two pre-contrast measurements of the same sequence at a variable flip angle (2° and 15°). The contrast agent administration (0.2 ml/kg body weight) was done with a flow-rate of 3.5 ml/s, followed by saline flush, using a power injector.

In addition, after dynamic acquisitions, a volume Interpolated GRE isotropic at high resolution and a T1-weighted turbo spin echo with fat suppression were acquired.

Table 1 shows technical details of the above-mentioned MR sequences.

In order to obtain good MRI image quality, all patients were carefully instructed to refrain from vigorous swallowing or breathing during image acquisition especially during the acquisition of DWI sequences. Small breaks were made between individual sequences to allow patients to clear the throat of mucous secretions, cough, or swallow.

2.7. Data processing and multiparametric analysis

PET data obtained simultaneously with CT and MR examination were processed with comparable reconstruction and correction algorithms. For both modalities, emission data were corrected for randoms, dead time, scatter, and attenuation.

Tumor tissue was identified as any voxel in the 3D dataset with counts greater than a fixed threshold fraction of the peak activity in the tumor. The threshold level for tumor characterization was selected as a Standardized Uptake Value (SUV) equal to or higher than 3.5 [16]. The SUVs were calculated automatically by the software (Syngo.via, Siemens Medical Systems) using the body weight method: SUV = [decay corrected tissue activity (kBq/ml)]/[injected 18F-FDG dose per body weight (kBq/g)]. The maximum SUV (SUVmax) and mean SUV (SUVmean) of the tumor tissue were derived automatically by the software using a voxel-of-interest (VOI) method of tissue delineation for both the acquisitions. Moreover, based on SUV values, a volumetric characterization of lesion burden was made as suggested in a previous study [17] considering a metabolic tumor volume (MTV) with a threshold of 40% of the maximum signal intensity (MTV40).

Two groups of one senior radiologist experienced in head and neck imaging (8 and 10 years experience) and one nuclear medicine specialist (9 and 7 years experience) were blinded to the PET/CT findings and consensually reviewed tumor findings on PET/MR images in consensus. Primary tumor size and infiltration of neighboring structures were assessed (Fig. 1A). A comparison between PET/CT and PET/MR findings has not been performed considering that CT examination was without contrast agent injection and this could bias the analysis by underestimating CT diagnostic accuracy (Fig. 1B).

Subsequently, the DCE-MR images were transferred for post-processing to a workstation running commercially available software for tissue perfusion estimation (Tissue 4D, Siemens Medical Systems). After motion correction and registration of the pre- and post-contrast acquisitions, T1 mapping was automatically performed and a freehand region-of-interest (ROI) was plotted around the tumor including the neighboring vessels (carotid arteries, jugular vein). The pharmacokinetic modeling was based on a two-compartment model that allows for the calculation of the following: transfer constant between vascular, extravascular, and extracellular space (EES) (K^{trans}); the volume of EES (v_e); the constant between EES and blood plasma (k_{ep}); the initial area under the concentration curve (iAUC) [18]. K^{trans} is a parameter related to vessel permeability and tissue blood flow. The leakage space V_e is a marker of cell density, the k_{ep} is a transfer constant from the extracellular/extravascular space to plasma, and iAUC is related to the blood volume in the tissue of interest [18]. Arterial input function (AIF) was related to gadolinium dose injected and was modeled by a bi-exponential function using an intermediate mode provided by the software. For the subsequent tumor ROI analysis, PET/MR datasets (PET acquisition, axial T1 post-contrast and axial T2 sequences, axial ADC map, and single perfusion maps for K^{trans}, v_e, k_{ep} and iAUC) were evaluated into a unified measurements framework customized into the Syngo.via software platform (Siemens Medical Solutions) allowing a visual comparison of the multiparametric data. Post-contrast T1-weighted as well as T2-weighted images were utilized to drive the tumor outline in major diameter lesion slice, which avoids necrotic areas and large feeding vessels. Therefore, ROI area value, referred as the tumor size in the major diameter lesion slice was extracted for each patient. For multiparametric comparisons, the ROI outline was drawn with the same position and extent on each map to automatically extract maximum and mean values for each parameter (SUVmax and SUVmean for the PET; ADCmax and ADCmean for the diffusion; K^{trans}, k_{ep}, v_e, and iAUC, respectively max and mean for perfusion maps) (Fig. 1A).

Table 1
Summary of MR acquisition protocol and sequences.

Sequence name	Orientation	Repetition time (ms)	Echo time (ms)	Flip angle (°)	Voxel size (mm^3)	Acquisition time (min:s)
STIR	Coronal	5000	84	125	1.1 × 0.8 × 3.5	2:02
FSE T2-w	Axial	5000	117	90	0.7 × 0.7 × 3.0	3:10
FSE T1-w	Axial	590	9.9	150	0.9 × 0.6 × 3.0	4:32
DWI	Axial	13,800	70		2.8 × 2.8 × 4.0	2:11
Volume Interpolated GRE	Axial	5.37	1.78	15	1.7 × 1.2 × 3.6	0:10
Volume Interpolated GRE ISO	Axial	4.93	2.29	9	1 × 1 × 1	4:41
TSE FAT SAT T1-w	Axial	5.79	8.5	138	0.8 × 0.6 × 3	3:58

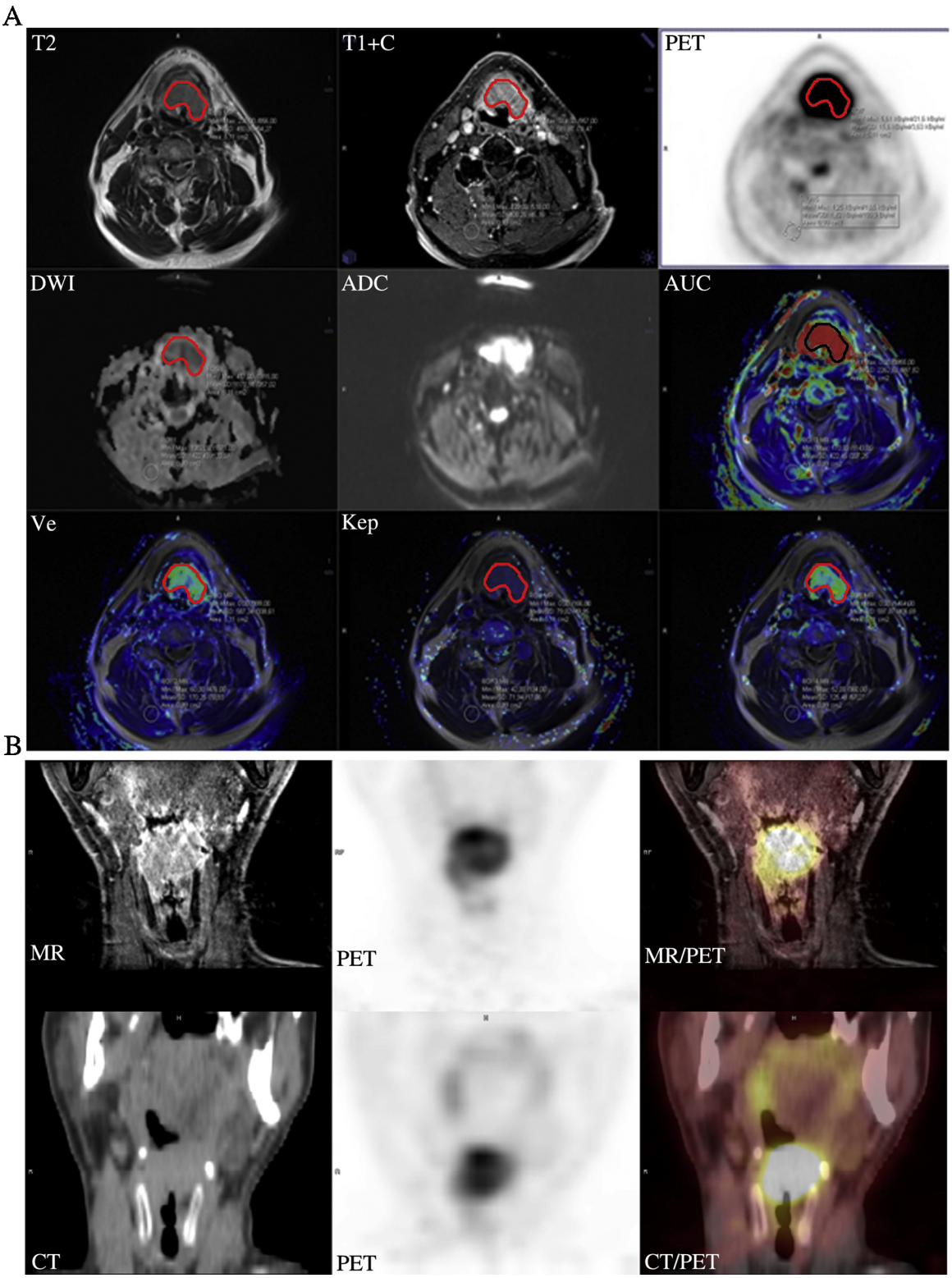

Fig. 1. In A, ROI placement for multiparametric analysis in a 70 y.o. male with HNSCC lesion in primary staging. ROI (in red) was manually outlined on post-contrast T1-weighted (T1 + C) and T2-weighted (T2) images in major diameter lesion slice, and following drawn with same position and extent on each map. In B, a coronal view of the same patient from both PET/MR and PET/CT acquisitions.

Moreover, standardized ROIs ($1\,cm^2$) were placed in the paraspinal muscle of each patient in order to obtain SUV, ADC, and DCE-MRI estimates in the normal tissue and provide significant differences compared with the tumor tissue.

2.8. Statistical analysis

Multiparametric data were exported and analyzed using the Sigmaplot v10.0 program with Sigma-Stat integration v3.2 (SPSS,

Erkrath, Germany). A p-value of less than 0.05 was considered statistically significant. The values are presented as mean ± standard deviation (SD).

The Kolmogorov–Smirnov test was first used to examine if the data was normally distributed. Cohen's kappa was used to evaluate agreement for primary tumor detection in PET/MR between the two groups of observers, without accounting for lymph nodes involvement and putative distant metastases. Any differences in the parameters estimations between the normal and tumor tissue and between the primary tumors and recurrent lesions were determined with a t-student test. Spearman's correlation coefficients were calculated to compare MRI and CT based SUV values and to compare metabolic diffusion and perfusion parameters. A correlation coefficient ρ of ≤0.35 was considered low, 0.36–0.67 moderate, 0.68–0.90 high, and ≥0.90 to be excellent correlations [19].

3. Results

3.1. Feasibility and interobserver agreement

All PET/CT and PET/MR studies were acquired successfully and were suitable for further evaluation.

Satisfactory agreement between the two observer groups was found in anatomic allocation of lesions by PET/MR (T-staging) with no significant differences between the two clinically defined groups (Primary tumors: 97%, Cohen's kappa 0.93; Recurrent tumors: 93%, Cohen's kappa 0.89).

3.2. Multiparametric comparison in the overall sample and subgroups definition

The summary statistics for the FDG-metabolism, diffusion, and perfusion measurements in the healthy muscle tissue and the tumors are demonstrated in Table 2.

Representative cases of multiparametric head–neck imaging are shown in Figs. 2 and 3.

When grouping all patients together (n = 44) there was a significant positive correlations between the ROI area, the SUV measures, and the SUV estimations. Conversely, there was a significant negative correlation between MR SUV ROI, and ADC Mean. There was also a significant negative correlation between ADC Mean and K^{trans} Mean (Table 3).

In particular, there were two subgroups identified for patients in primary or recurrent tumors. Primary tumors (n = 22) included 11 laryngeal, 3 oral, 1 sinonasal, 2 oropharingeal, 3 parotid, and 2 rhinopharingeal cancers.

Recurrent tumors (n = 22) included 14 cases of laryngeal, 3 oral, 2 sinonasal, 1 parotid, and 2 rhinopharingeal cancers. In particular, 11 patients received only surgical treatment, 4 radiotherapy, and 7 both chemo- and radiotherapy.

3.3. Multiparametric comparison in primary tumors

As for as primary tumors the correlation analysis demonstrated a significant correlation between the ROI area, the SUV measures, and the SUV estimations.

Conversely, there was a significant negative correlation between ADC Mean and K^{trans} Mean (Fig. 2; Table 3).

3.4. Multiparametric comparison in recurrent tumors

As for as recurrent tumors, the Spearman's ρ coefficient analysis among the different parameters in the tumor sites demonstrated a significant correlation between the ROI area and the MR SUV ROI. However, the correlation was not significant with CT SUV VOI or MR SUV VOI (p = 0.35 and .23, respectively), which was demonstrated in primary tumors. A significant correlation was also found between the SUV measures, MR SUV VOI, and MR SUV ROI. Finally, a significant negative correlation was found between MR SUV ROI and ADC mean (Fig. 3; Table 3).

No significant differences were detected between the two groups for metabolic, diffusion and perfusion parameters. SUV estimation and all perfusion parameters (K^{trans}, k_{ep}, v_e, and iAUC) in tumors were significantly higher compared to normal muscle tissue in both the groups (Primary tumors: p < 0.001; Recurrent tumors p < 0.001) (Figs. 1 and 2, Table 2). Conversely, the ADC mean value in tumors was significantly lower compared to normal paraspinal

Table 2
Summary of metabolic, diffusion and perfusion parameters in both the groups.

Parameter	Overall sample		Primary tumors		Recurrent tumors		Muscle	
	Mean	SD	Mean	SD	Mean	SD	Mean	SD
AGE	60.94	2.23	62.52	12.35	59.36	12.93		
AREA – Tumor size (cm^2)	2.73	0.37	2.99	4.90	2.47	1.73	1	0
CT SUV Mean	5.77	1.76	4.53	4.53	7.01	5.75	0.715**	0.065
CT MTV (cm^3)	14.42	1.62	15.56	19.48	13.27	14.24		
MR SUV Mean	7.78	2.39	6.09	5.05	9.47	8.91	0.721**	0.077
MR MTV (cm^3)	11.92	1.58	13.03	16.59	10.81	11.78		
SUV Mean 2D	20.36	1.35	19.40	24.10	21.32	17.66	0.724**	0.079
ADC Mean ($\mu m^2/s$)	1193.26	0.14	1193.14	481.68	1193.4	187.09	1483.58*	108.2
K^{trans} Mean (min^{-1}) (×1000)	268.09	13.60	277.71	167.29	258.48	150.82	51.18*	10.36
k_{ep} MEAN (min^{-1}) (×100)	83.99	5.98	88.22	62.30	79.76	31.73	51.59*	14.36
iAUC Mean (mM min) (×50)	901.54	17.73	914.08	472.24	889.01	539.96	166.21*	30.27
v_e Mean (×1000)	326.35	25.84	308.08	124.99	344.62	133.11	103.52*	22.03

Abbreviations: CT: computed tomography; SUV: standardized uptake value; MR: magnetic resonance; MTV: metabolic tumor volume; ADC: apparent diffusion coefficient; K^{trans}: transfer constant between vascular and EES; k_{ep}: constant between EES and blood plasma; iAUC: initial area under the concentration curve in 60 s; v_e: the volume of EES per unit of volume of tissue.

* $p \leq 0.05$;
** $p \leq 0.01$.

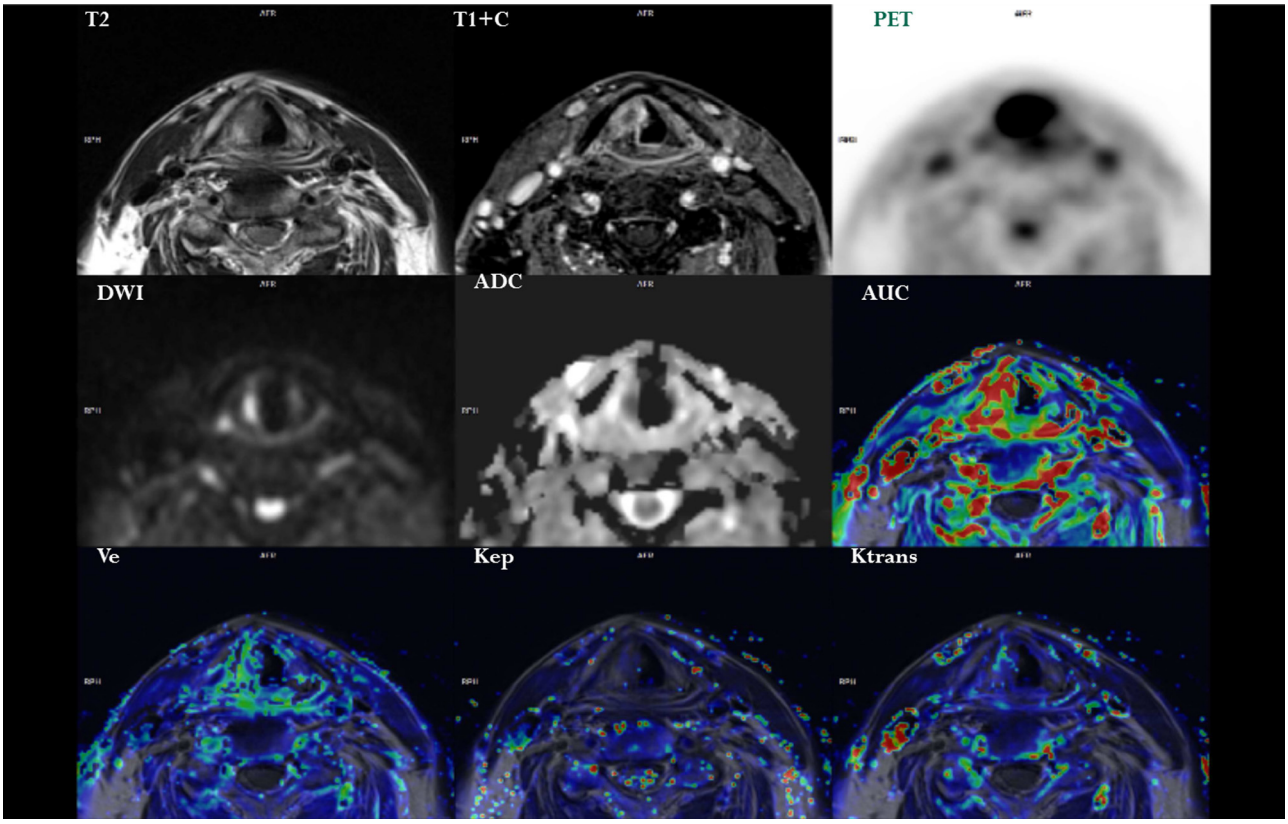

Fig. 2. Multiparametric evaluation of morphological (T1, and T1 + C), metabolic (PET) and functional (DWI, ADC, iAUC, v_e, k_{ep}, and K^{trans}) in a 57 y.o male with right vocal cord HNSCC and anterior commissure infiltration in primary staging. The increase of thickness and enhancement of the tumor site in the morphological acquisitions, the increase of FDG-uptake, and the reduced diffusivity in ADC with an increase of perfusion parameters were detected.

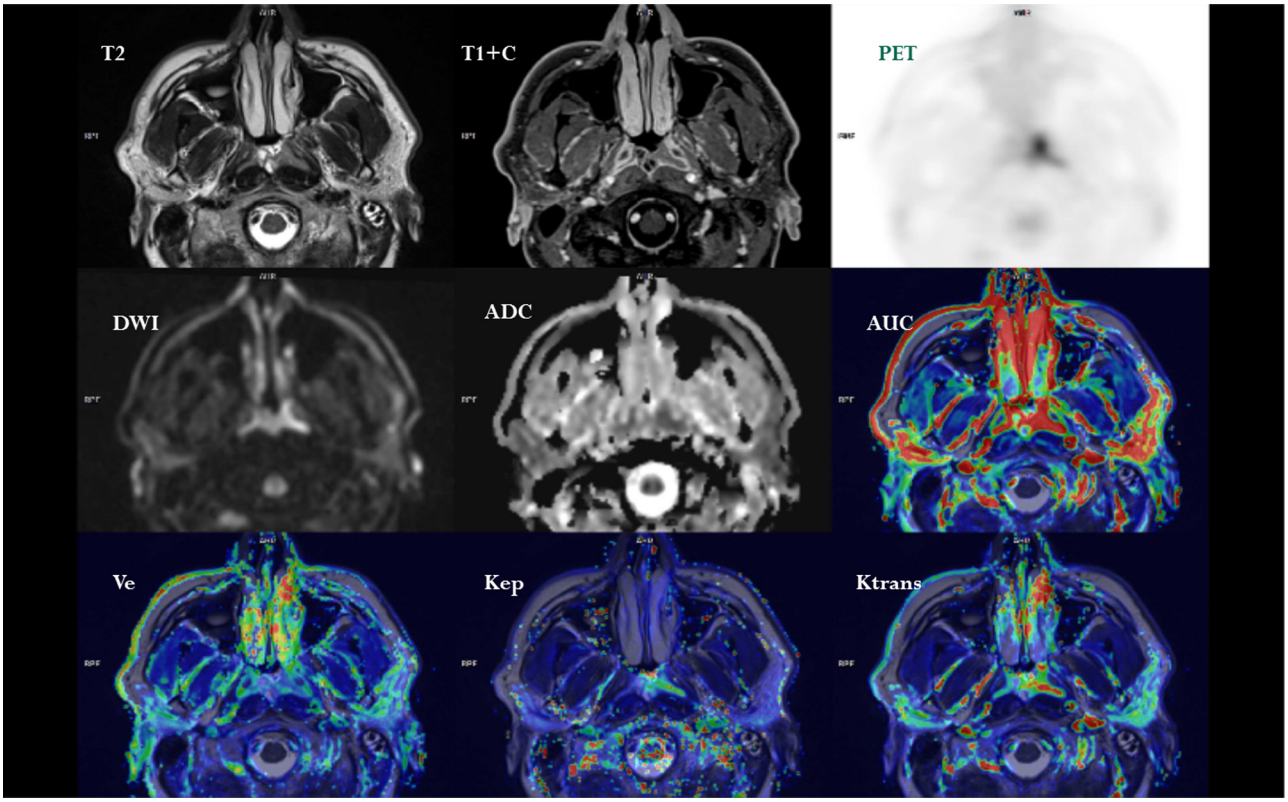

Fig. 3. Multiparametric evaluation of morphological (T1, and T1 + C), metabolic (PET) and functional (DWI, ADC, iAUC, v_e, k_{ep}, and K^{trans}) in a 69 y.o. male recurrency after surgery for a HNSCC of the larynx. The increase of thickness and enhancement of the tumor site in the morphological acquisitions, the increase of FDG-uptake, and the reduced diffusivity in ADC with an increase of perfusion parameters were detected.

Table 3
Significant correlations in multiparametric analysis.

Parameters	Spearman's ρ coefficient	Significance (p value)
Overall sample		
ROI area vs. CT SUV VOI	0.66	<0.001
ROI area vs. MR SUV VOI	0.61	<0.001
ROI area vs.MR SUV ROI	0.61	<0.001
CT SUV VOI vs. MR SUV VOI	0.97	<0.001
CT SUV VOI vs. MR SUV ROI	0.88	<0.001
MR SUV VOI vs. MR SUV ROI	0.91	<0.001
CT MTV vs. MR MTV	0.94	<0.001
MR SUV ROI vs. ADC Mean	−0.36	0.04
ADC Mean vs. K^{trans} Mean	−0.5	<0.001
Primary tumors		
ROI area vs. CT SUV VOI	0.51	0.04
ROI area vs. MR SUV VOI	0.45	0.04
ROI area vs. MR SUV ROI	0.53	0.01
CT SUV VOI vs. MR SUV VOI	0.95	<0.001
CT SUV VOI vs. MR SUV ROI	0.81	<0.001
MR SUV VOI vs. MR SUV ROI	0.83	<0.001
CT MTV vs. MR MTV	0.93	<0.001
ADC Mean vs. K^{trans} Mean	−0.42	0.04
Recurrent tumors		
ROI area vs. MR SUV ROI	0.61	0.04
MR SUV VOI vs. MR SUV ROI	0.99	0.01
MR SUV ROI vs. ADC mean	−0.72	0.01

Abbreviations: ROI area: tumor size in 2D major lesion size; *Abbreviations*: CT: computed tomography; SUV: standardized uptake value; MTV: metabolic tumor volume; ADC: apparent diffusion coefficient; K^{trans}: transfer constant between vascular and EES.

muscle (Primary tumors: $p < 0.001$; Recurrent tumors: $p < 0.001$) (Table 2).

4. Discussion

This study demonstrated the feasibility of PET/MR examination for the evaluation of the T-stadium in patients with head and neck cancer during staging or follow-up. This study also found PET/MR examination to have a high inter-observer agreement for lesion detection and significant relationships among several metabolic, diffusion, and perfusion parameters in the primary tumor.

In the past three decades PET has demonstrated its value in providing non-invasive information of tissue at the molecular level. The value of PET lies in its high sensitivity tracking of in vivo biomarkers, however it lacks precise anatomical information, which has been overcome with the introduction of the PET/CT scanners. 18F-labeled fluorodeoxyglucose positron emission tomography ([18F]FDG PET) is commonly used in HNSCC for tumor staging, monitoring of treatment responses, detection of recurrences, and radiotherapy planning [5]. Although PET/CT is currently the gold standard for oncological imaging, several limitations exist, which include: substantial amounts of ionizing radiation from repeated PET/CT scans during diagnostic and follow-up examinations; the anatomical contribution of CT is limited in soft tissues and areas with complex anatomy (i.e. the head and neck & pelvis region).

These issues can be overcome with recently launched fully integrated hybrid PET/MR scanners, which can perform simultaneous acquisition of PET and MRI. By combining anatomical MRI, DW-MRI, DCE-MRI and PET imaging to obtain concerted information about cellularity, perfusion and biological activity of the tumor (i.e. by use of FDG, FLT or Choline), we hypothesize that the sensitivity and the specificity in oncology staging can be improved. However, currently no specific clinical indication for PET/MR has been established.

PET/CT and PET/MR studies were acquired in all 44 patients without side effects and were suitable for further evaluation. Although several studies have demonstrated the feasibility of this new powerful tool in oncological imaging, the head and neck region includes complex anatomy with many different tissues in a small region and is often affected by involuntary motion artifacts during imaging acquisition. The ability to perform simultaneous acquisition decreases the acquisition time bypassing putative co-registration problems, especially for high-temporal resolution phenomena like perfusion.

Indeed, software fusion of PET and MRI data is challenging in the neck and the simultaneous acquisition of the MRI and PET data provides improved coregistration. The feasibility of PET/MR in the head and neck region has also been reported by other groups, demonstrating a good MR image quality without impairment of the PET signal [20,21].

The high contrast resolution of MRI compared to CT created a more fine differentiation of head and neck tissues, which provided a correct staging and follow-up of HNSCC, mainly for T stadium characterization [10]. A recent article that examined thirty patients with HNC cancer at primary tumors found a higher diagnostic accuracy for T evaluations from retrospectively fused PET/MR compared to PET/CT and a comparable accuracy for N-staging [22]. Our current study also supports this previous report by demonstrating excellent agreement between the two observer groups for the anatomic allocation of lesions by PET/MR (T-staging). This has also been found in other studies, examining different types of cancer (lymph nodes and distant metastases) revealing inter-reader agreement between observers of about 0.5 [23] and 0.7 [24].

As for the correlation analysis, there was a significant positive relationship between the ROI area (tumor size in the major axial lesion diameter) and the SUV. This correlation shows that bigger lesions have higher metabolic activity, although the presence of necrotic intralesional regions can bias SUV estimation. In this study, we limit this bias performing a manual tumor outline in major diameter lesion slice, avoiding necrotic areas and large feeding vessels. Although there are controversial results with respect to the correlation between the lesion size and SUV measurement [25,26] the differences found between primary and recurrent tumors could be alsodue to the effect of different therapies on lesion homogeneity. Fruehwald-Pallamar et al. [26] reported no significant differences in ADC values and SUVmax between the various T stages in 31 patients. The possible inclusion of inflammation, fibrosis and/or necrosis within the ROI lesion area measured along the major axis is a likely consequence of surgery, radiotherapy, chemotherapy or different combined therapeutic approaches during the follow-up. For these reasons, in order to reduce effects related to treatments, 6–8 weeks from the end of treatment passed before the imaging study of recurrent lesions. Also previous reports and the current study have found comparable estimates of metabolic parameters (SUV and MTV) between PET/CT and PET/MR mainly in primary tumors and the overall sample. In a recent report [23], a very high correlation between the SUV value in 18F-FDG-PET/MR and 18F-FDG-PET/CT imaging has been detected for primary tumors, lymph node, and distant metastases in 14 patients. Other authors [12,24] found no statistically significant difference in diagnostic capability between PET/CT and PET/MR in 17 patients. Although MRI-based AC is still under debate [14], 2-point Dixon approach for MRI attenuation has recently provided results comparable to those of conventional attenuation correction by low dose CT [12]. High correlation between SUV estimated by PET/CT and PET/MR resulting from this study supports these conclusions, according to a previous work [14]. In the current study when examining metabolic (SUV), diffusion (ADC) and perfusion parameters (K^{trans}, k_{ep}, iAUC, v_e), we demonstrated a significant negative correlation between MR SUV ROI and ADC Mean in recurrent tumors and the overall sample. Although the cell density (estimated by ADC) and glucose metabolism (estimated by SUV) of a tumor are different physiological parameters, one recent report has shown a positive correlation between SUV max and ADC values [27]. Other studies

[26,28] have observed no significant correlation between these two parameters with MRI and PET/CT. The negative correlation resulting from this study shows that higher cellularity of the lesions, reflecting on a low ADC, parallels with an increased glucose uptake and cellular metabolism. Controversial results [26–28], instead, can be due to tumor inhomogeneity and contextual necrotic areas, where the free diffusion of water protons results in no ADC restriction [26].

In addition, there was a significant negative correlation between ADC Mean and K^{trans} Mean in primary tumors and the overall sample. Although few studies have investigated the relationship among these parameters, the results appear controversial [26–28]. An inverse correlation between ADC and K^{trans} has also been detected for other tumors (i.e. brain) [27], which suggests an intricate relationship between vascular permeability and the tumor microenvironment. In this context, two tumoral features may explain the negative correlation between these parameters. From one side, tumor proliferation increases cell density and ADC restriction while, from the other hand, neoangiogenesis increases immature tumoral vessels and, thereby, vascular permeability expressed by K^{trans}.

Finally, perfusion parameters such as K^{trans} have been demonstrated to be potentially predictive of patient response to therapy, however controversial results can be debated [29]. Any differences may be attributed to the applied pharmacokinetic modelling (e.g. (extended) Tofts model or more elaborated models like the shutter-speed one) [18]. In any case, Ktrans seems to be suitable to monitor therapy (relative) changes in tumors though the correctness of the absolute values may be not always claimed [30].

5. Conclusions

Our study demonstrates the feasibility of PET/MR imaging in the T-stadium evaluation of HNC lesions during staging or follow-up. This introduces a more complete characterization of metabolic, diffusion, and perfusion characteristics of primary lesions.

The strength and the originality of this study exists in the involvement of multiparametric MRI, which include both diffusion and perfusion evaluations that are collected simultaneously during PET/MR acquisition.

Although further improvements should be performed to increase the value of hybrid acquisition of PET/MR (improved attenuation correction algorithm for bone segmentation, and surface dedicated coils for head and neck region), we believe this analysis may play a crucial role in prognosis and treatment of patients when considering the predictive value of these parameters [29].

Conflict of interest

All authors have no conflicts of interest and no disclosures of financial interest to report.

References

[1] Jansen JFA, Koutchger JA, Shukla-Dave A. Non-invasive imaging of angiogenesis in head and neck squamous cell carcinoma. Angiogenesis 2010;13(2):149–60.

[2] Shang J, Gu J, Han Q, Xu Y, Yu X, Wang K. Chemoradiotherapy is superior to radiotherapy alone after surgery in advanced squamous cell carcinoma of the head and neck: a systematic review and meta-analysis. Int J Clin Exp Med 2014;7:2478–87.

[3] Schoder H, Fury M, Lee N, Kraus D. PET monitoring of therapy response in head and neck squamous cell carcinoma. J Nucl Med 2009;50:74S–88S.

[4] Cooper JS, Pajak TF, Forastiere AA, Jacobs J, Campbell BH, Saxman SB, et al. Postoperative concurrent radiotherapy and chemotherapy for high-risk squamous-cell carcinoma of the head and neck. N Engl J Med 2004;350:1937–44.

[5] Bernier J, Domenge C, Ozsahin M, Matuszewska K, Lefèbvre J-L, Greiner, RH, et al. Postoperative irradiation with or without concomitant chemotherapy for locally advanced head and neck cancer. N Engl J Med 2004;350:1945–52.

[6] Vandecaveye V, Dirix P, De Keyzer F, de Beeck KO, Vander Poorten V, Roebben I, et al. Predictive value of diffusion weighted magnetic resonance imaging during chemoradiotherapy for head and neck squamous cell carcinoma. Eur Radiol 2010;20(7):1703–14.

[7] Chawla S, Kim S, Loevner LA, Hwang WT, Weinstein G, Chalian A, et al. Prediction of disease-free survival in patients with squamous cell carcinomas of the head and neck using dynamic contrast enhanced MR Imaging. AJNR Am J Neuroradiol 2011;32(4):778–84.

[8] Partovi S, Kohan A, Rubbert C, Vercher-Conejero JL, Gaeta C, Yuh R, et al. Clinical oncologic applications of PET/MRI: a new horizon. Am J Nucl Med Mol Imaging 2014;4(2):202–12.

[9] Partovi S, Robbin MR, Steinbach OC, Kohan A, Rubbert C, Vercher-Conejero JL, et al. Initial experience of MR/PET in a clinical cancer center. J Magn Res Imaging 2014;39:768–80.

[10] Buchbender C, Heusner TA, Lauenstein TC, Bochisch A, Antoch G. Oncologic PET/MRI. Part 1: tumors of the brain, head and neck, chest, abdomen and pelvis. J Nucl Med 2012;53:928–38.

[11] Surti S, Kuhn A, Werner ME, Perkins AE, Kolthammer J, Karp JS. Performance of Philips Gemini TF PET/CT scanner with special consideration for its time-of-flight imaging capabilities. J Nucl Med 2007;48(3):471–80.

[12] Seemann MD. Whole-body PET/MRI: the future in oncological imaging. Technol Cancer Res Treat 2005;4:577–82.

[13] Delso G, Furst S, Jackoby B, Ladebeck R, Ganter C, Nekolla SG, et al. Performance measurements of the Siemens mMR integrated whole-body PET/MR scanner. J Nucl Med 2011;52(12):1914–22.

[14] Varoquaux A, Rager O, Poncet A, Delattre BM, Ratib O, Becker CD, et al. Detection and quantification of focal uptake in head and neck tumours: 18F-FDG PET/MR versus PET/CT. Eur J Nucl Med Mol Imaging 2014;41(3):462–75.

[15] Arabi H, Rager O, Alem A, Varoquaux A, Becker M, Zaidi H. Clinical assessment of MR-guided 3-class and 4-class attenuation correction in PET/MR. Mol Imaging Biol 2014:1–13.

[16] Baek CH, Chung MK, Son YI, Choi JY, Kim HJ, Yim YJ, et al. Tumor volume assessment by 18F-FDG PET/CT in patients with oral cavity cancer with dental artifacts on CT or MR images. J Nucl Med 2008;49:1422–8.

[17] Erdi YE, Mawlawi O, Larson SM, Imbriaco M, Yeung H, Finn R, et al. Segmentation of lung lesion volume by adaptive positron emission tomography image thresholding. Cancer 1997;80:2505–9.

[18] Tofts PS, Kermode AG. Measurement of the blood-brain barrier permeability and leakage space using dynamic MR imaging 1. Fundamental concepts. Magn Reson Med 1991;17:357–67.

[19] Pace L, Nicolai E, Luongo, A, Aiello M, Catalano OA, Soricelli A, et al. Comparison of whole-body PET/CT and PET/MRI in breast cancer patients: lesions detection and quantification of 18F-deoxyglucose uptake in lesions and in normal organ tissues. Eur J Radiol 2014;83:289–96.

[20] Platzek I, Beuthien-Baumann B, Schneider M, Gudziol V, Langner J, Schramm G, et al. PET/MRI in head and neck cancer: initial experience. Eur J Nucl Med Mol Imaging 2013;40:6–11.

[21] Boss A, Stegger L, Bisdas S, Kolb A, Schwenzer N, Pfister M, et al. Feasibility of simultaneous PET/MR imaging in the head and upper neck area. Eur Radiol 2011;21:1439–46.

[22] Kanada T, Kitajima K, Suenaga Y, Konishi J, Sasaki R, Morimoto K, et al. Value of retrospective image fusion of 18F-FDG PET and MRI for preoperative staging of head and neck cancer: comparison with PET/CT and contrast-enhanced neck MRI. Eur J Radiol 2013;82:2005–10.

[23] Patrovi S, Kohan A, Vercher-Conejero JL, Rubbert C, Margevicius S, Schluchter MD, et al. Qualitative and quantitative performance of 18F-FDG-PET/MRI versus 18F-FDG-PET/CT in patients with head and neck cancer. AJNR Am J Neuroradiol 2014;35(10):1970–5.

[24] Kubiessa K, Purz S, Gawlitza M, Kuhn A, Fuchs J, Steinhoff KG, et al. Initial clinical results of simultaneous 18F-FDG PET/MRI in comparison to 18F-FDG PET/CT in patiens with head and neck cancer. Eur J Nucl Med Mol Imaging 2014;41:639–48.

[25] Khalaf M, Abdel-Nabi H, Baker J, Shao Y, Lamonica D, Gona J. Relation between nodule size and 18F-FDG-PET SUV for malignant and benign pulmonary nodules. J Hematol Oncol 2008;1:13, http://dx.doi.org/10.1186/1756-8722-1-13.

[26] Fruehwald-Pallamar J, Czerny C, Mayerhoefer ME, Halpern BS, Heder-Czembirek C, Brunner M, et al. Functional imaging in headand neck squamous cell carcinoma: correlation of PET/CT and diffusion-weighted imaging at 3 Tesla. Eur J Nucl Med Mol Imaging 2011;38(6):1009–19.

[27] Chu JP, Mak HK, Yau KK, Zhang L, Tsang J, Chan Q, et al. Pilot study on evaluation of any correlation between MR perfusion (Ktrans) and diffusion (apparent diffusion coefficient) parameters in brain tumors at 3 Tesla. Cancer Imaging 2012;12:1–6, http://dx.doi.org/10.1102/1470-7330.2012.0001.

[28] Varoquaux A, Rager O, Lovblad K-O, Masterson K, Dulquerov P, Ratib O, et al. Functional imaging of head and neck squamous cell carcinoma with diffusion-weighted MRI and FDG PET/CT: quantitative analysis of ADC and SUV. Eur J Nucl Med Mol Imaging 2013;40(6):842–52.

[29] Bernstein JM, Homer JJ, West CM. Dynamic contrast-enhanced magnetic resonance imaging biomarkers in head and neck cancer: potential to guide treatment? A systematic review. Oral oncology 2014 Oct;50(10):963–70.

[30] Bisdas S, Smrdel U, Bajrovic FF, Surlan-Popovic K. Assessment of progression-free-survival in glioblastomas by intratreatment dynamic contrast-enhanced MRI. Clin Neuroradiol 2014;(August), http://dx.doi.org/10.1007/s00062-014-0328-0.